Supplementary material for joint regional uptake quantification of ^{227}Th and ^{223}Ra using a multiple-energy-window projection-domain quantitative SPECT method

1. Image reconstruction-based methods compared

In this section, we present the two image-reconstruction methods that were compared with the proposed multiple-energy-window projection-domain quantitative (MEW-PDQ) SPECT method.

1.1 Dual-isotope ordered subset expectation maximization image reconstruction (DOSEM)-based method

The DOSEM-based method that we developed for our comparison study was inspired by and similar to a quantitative ^{227}Th SPECT reconstruction method proposed by Ghaly et al. [1]. This method, in turn, advances upon a method proposed for simultaneous ^{99m}Tc and ^{123}I dual-isotope SPECT [2]. In brief, the method frames the inverse problem of ^{227}Th SPECT reconstruction as a dual-isotope reconstruction problem where the two isotopes are ^{227}Th and ^{223}Ra. Reconstruction is then conducted through an iterative process that models the crosstalk of the two isotopes as well as the other SPECT image-degrading artifacts.

In the developed method, we first independently reconstructed images of activity uptake of ^{227}Th and ^{223}Ra using projections from the corresponding two separate primary energy windows, namely, 215 - 260 keV and 75 - 100 keV, respectively. These two energy windows were chosen since they corresponded to the major photopeaks for these isotopes and had the highest number of detected events for these two isotopes. The images were reconstructed using the ordered subset expectation maximization (OSEM) method, implemented using Customizable and Advanced Software for Tomographic Reconstruction (CASToR) software [3]. The reconstruction compensated for attenuation, scatter, collimator-detector response, stray-radiation-related noise, and the complicated emission spectra of both isotopes. The scatter was compensated using the effective scatter source estimation (ESSE) method [4]. Next, the reconstructed image for each isotope was forward projected to the photopeak energy window of the other isotope to estimate the crosstalk contamination in each photopeak energy window. In this forward projection, we modeled the emission spectra of both isotopes, along with the attenuation, scatter, and collimator-detector response. In this step, the crosstalk contamination from primary photons was modeled from the emission spectrum, and the crosstalk contamination from scattered photons was modeled with the ESSE method. Following this process, the images of both isotopes were again reconstructed using the OSEM method, with the estimated crosstalk contamination as additive correction terms. The process was repeated iteratively until the changes in the reconstructed images were small. With this process, we reconstructed separate images for

^{227}Th and ^{223}Ra. Finally, the regional activity uptake of each isotope were estimated by averaging all the voxel in the corresponding image within the volumes of interest (VOIs).

1.2 Geometric transfer matrix (GTM)-based method

Partial volume effects (PVEs) are known to degrade quantification accuracy in SPECT [5]. The MEW-PDQ method implicitly assumes constant uptake within each VOI. Under this assumption, PVEs can also be compensated as a post-reconstruction step. A widely used approach for this purpose is the GTM-based method [6], and thus we used this method to compensate for the PVEs in the estimated regional uptake obtained by the DOSEM-based method as a comparison study.

We compensated for the PVEs of the estimated regional uptake of ^{227}Th and ^{223}Ra independently, but followed the same process. Considering one of the isotopes, the GTM-based method required computing the elements of a geometric transfer matrix. For this purpose, we first obtained the projections of each VOI with unit activity uptake of the isotope in the corresponding primary energy window, using our SIMIND-based simulation approach. We then reconstructed the projections of each VOI using the OSEM method. These reconstructed images provided the regional spread function (RSF) of each VOI for imaging the isotope of interest. With the RSFs, the elements of the geometric transfer matrix were computed as described in [6]. Applying the inverse of the geometric transfer matrix to the estimated regional uptake values of the considered isotope yielded the estimates with the GTM-based method.

2. Figures of merit

For a range of experimental conditions, we generated multiple instances of projection data for a single phantom, where each instance corresponded to separate noise realizations. Denote the total number of realizations by R. Considering one of the isotopes, denote the true activity uptake of the k^{th} VOI by λ_k and the corresponding estimate with the r^{th} noise realization by $\hat{\lambda}_{rk}$. In these experiments, the accuracy of the estimated uptake of this isotope was quantified using the normalized bias (NB), which, for the k^{th} VOI, is given by

$$\mathrm{NB}_k = \frac{1}{R}\sum_{r=1}^{R}\frac{\hat{\lambda}_{rk}-\lambda_k}{\lambda_k}. \qquad (1)$$

The precision of the estimated uptake of this isotope was quantified using the normalized standard deviation (NSD), which, for the k^{th} VOI, is given by

$$\mathrm{NSD}_k = \sqrt{\frac{1}{R-1}\sum_{r=1}^{R}\left(\frac{\hat{\lambda}_{rk}}{\lambda_k}-\frac{1}{R}\sum_{r\prime=1}^{R}\frac{\hat{\lambda}_{r\prime k}}{\lambda_k}\right)^2}. \qquad (2)$$

Finally, the overall error in estimating the uptake was quantified by the normalized root mean square error (NRMSE). For the k^{th} VOI,

$$\text{NRMSE}_k = \sqrt{NB_k^2 + NSD_k^2}. \qquad (3)$$

To evaluate the performance of the methods over populations, we used the ensemble NB and ensemble NRMSE. Denote the number of samples in the population by S and the true and estimated activity uptake of a particular isotope in the k^{th} VOI for the s^{th} sample by λ_{sk} and $\hat{\lambda}_{sk}$, respectively. The ensemble NB for the k^{th} VOI is given by

$$\text{Ensemble NB}_k = \frac{1}{S}\sum_{s=1}^{S}\frac{\hat{\lambda}_{sk} - \lambda_{sk}}{\lambda_{sk}}. \qquad (4)$$

The ensemble NRMSE for the k^{th} VOI is given by

$$\text{Ensemble NRMSE}_k = \sqrt{\frac{1}{S}\sum_{s=1}^{S}\left(\frac{\hat{\lambda}_{sk} - \lambda_{sk}}{\lambda_{sk}}\right)^2}. \qquad (5)$$

Additionally, to quantify performance in cases where we had just a single estimate, we used normalized error, defined as the difference between the true and estimated uptake values, normalized by the true uptake value.

Finally, we also computed the Cramér-Rao lower bound (CRLB), which is the minimum variance that can be achieved by an unbiased estimator, as a benchmark for the precision of the activity estimated using the proposed method. The CRLB is given by the diagonal elements of the inverse of the Fisher information matrix for the estimated parameter. We denote the Fisher information matrix by **F** [7]. Since the proposed method estimates the regional uptake of ^{227}Th and ^{223}Ra at the same time, the Fisher information matrix needs to consider both isotopes. We denoted λ_l and $\hat{\lambda}_l$ as the true and estimated activity uptake respectively, where l ranges over the two isotopes in K VOIs. Thus the Fisher information matrix is a $2K$ by $2K$ matrix with elements given by

$$F_{l_1 l_2} = -E\left[\frac{\partial^2}{\partial\lambda_{l_1}\,\partial\lambda_{l_2}}\ln\Pr(\mathbf{g}|\boldsymbol{\lambda})\right]. \qquad (6)$$

We have already derived the likelihood of the measured data **g** in the main material:

$$\Pr(\mathbf{g}|\boldsymbol{\lambda}) \quad = \prod_{m=1}^{M}\exp\left[-(\mathbf{H}\boldsymbol{\lambda})_m - \psi_m\right]\frac{[(\mathbf{H}\boldsymbol{\lambda})_m + \psi_m]^{g_m}}{g_m!}. \qquad (7)$$

Substituting Eq. (7) in Eq. (6) yields

$$F_{l_1 l_2} = \sum_{m=1}^{M}\frac{H_{ml_1}H_{ml_2}}{(\mathbf{H}\boldsymbol{\lambda})_m + \psi_m}. \qquad (8)$$

3. Validating the SPECT simulation

In our previous study [8], we demonstrated the accuracy of simulating ^{223}Ra SPECT with our SIMIND-based simulation approach. In this section, we validate the accuracy of our simulation approach on the task of simulating ^{227}Th SPECT, accounting for the emission from ^{223}Ra. To achieve this, we compared the projections of a physical phantom acquired from an actual scanner with those obtained using our simulation approach. We first outline the experimental design that we employed to validate our simulation approach, and subsequently present the results obtained from our experiments.

3.1 Experimental design to validate the simulation of ^{227}Th SPECT

We used SIMIND, a Monte Carlo-based approach, to model the SPECT imaging of the ^{227}Th isotope. SIMIND is a widely known approach that has already been shown to model SPECT imaging systems accurately [9]–[11], including when imaging other α-particle isotopes [8]. To demonstrate the accuracy of the SIMIND-based simulation approach for ^{227}Th-based α-RPT SPECT, we compared the projection data obtained with our simulation approach to that obtained on a physical scanner. For this purpose, we used a NEMA phantom (Data Spectrum^{TM}, USA). The spheres of this phantom were filled with ^{227}Th solutions with an activity concentration of 40 kBq/ml. The rest of the phantom was filled with water to simulate attenuation and scatter due to soft tissue. The phantom was scanned on a GE Discovery 670 SPECT/CT system with a medium energy general purpose (MEGP) collimator one day after purifying the ^{227}Th isotope and filling the isotope in the phantom. Thus, at the time of scanning, a small portion of the ^{227}Th had decayed to ^{223}Ra. During imaging, projections were acquired in two energy windows, corresponding to the two major photopeaks of ^{223}Ra (66 – 98 keV) and ^{227}Th (217 – 260 keV) at 60 angular positions spaced uniformly over 360°. This image-acquisition process was modeled using our simulation approach. In the simulation, the concentration of ^{227}Th and ^{223}Ra were calculated theoretically, based on the filling and scanning time. The profiles of the projection data obtained with the physical scanner and with the simulation approach from the two energy windows were compared.

3.2 Results

Fig. 1 shows projections of the NEMA phantom in the two energy windows at the first angular position, acquired using simulated and physical SPECT systems. We also compared the profiles along the dashed line in the projections from the two approaches in both energy windows. To reduce the noise-related variation in this profile, each point in the profile was obtained by averaging the number of counts along five adjacent pixels on both sides of the dashed line. We observed that the profile of the simulated projection matched that acquired on the physical scanner in both energy windows. This provides evidence of the accuracy of the process to simulate isotope emission, the SPECT system, and the noise in this study.

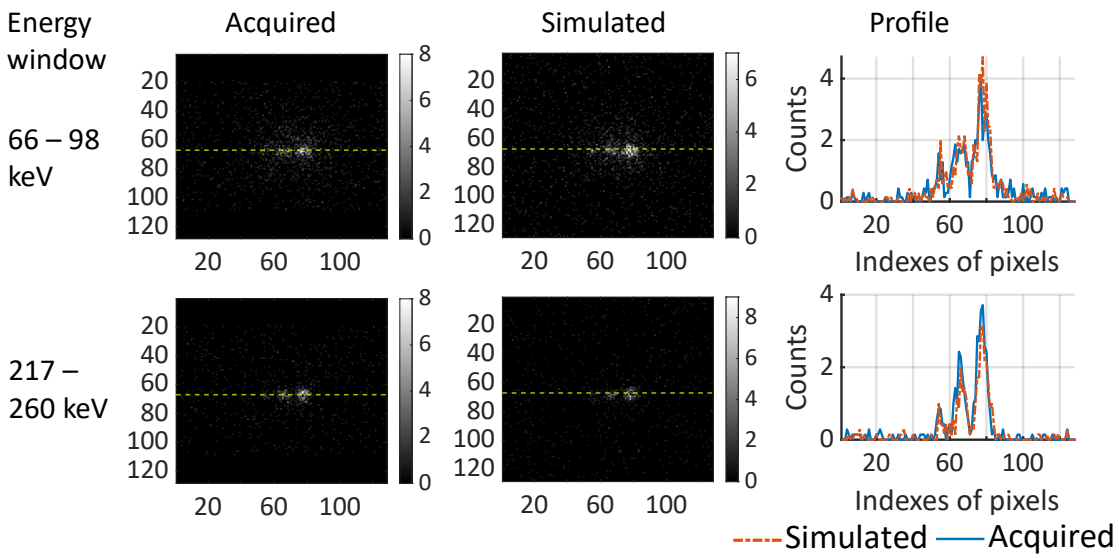

Figure 1: Comparison of the simulated and physical-SPECT-system-acquired projections of the NEMA phantom in two different energy windows.

[1] M. Ghaly, G. Sgouros, and E. Frey, "Quantitative Dual Isotope SPECT Imaging of the alpha-emitters Th-227 and Ra-223," J Nucl Med, vol. 60 (supplement 1), pp. 41–41, 2019.

[2] Y. Du, B. M. Tsui, and E. C. Frey, "Model-based crosstalk compensation for simultaneous dual-isotope brain SPECT imaging," Med Phys, vol. 34, no. 9, pp. 3530–3543, 2007.

[3] T. Merlin, S. Stute, D. Benoit, J. Bert, T. Carlier, C. Comtat, M. Filipovic, F. Lamare, and D. Visvikis, "CASToR: a generic data organization and processing code framework for multi-modal and multi-dimensional tomographic reconstruction," *Phys Med Biol*, vol. 63, no. 18, p. 185005, 2018.

[4] E. C. Frey and B. Tsui, "A new method for modeling the spatially-variant, object-dependent scatter response function in SPECT," in *1996 IEEE nucl sci symp conf rec*, 1996, vol. 2, pp. 1082–1086.

[5] M. Soret, S. L. Bacharach, and I. Buvat, "Partial-volume effect in PET tumor imaging," *J Nucl Med*, vol. 48, no. 6, pp. 932–945, 2007.

[6] O. G. Rousset, Y. Ma, and A. C. Evans, "Correction for partial volume effects in PET: principle and validation," *J Nucl Med*, vol. 39, no. 5, pp. 904–911, 1998.

[7] H. H. Barrett and K. J. Myers, *Foundations of image science*. John Wiley & Sons, 2013.

[8] Z. Li, N. Benabdallah, D. S. Abou, B. C. Baumann, F. Dehdashti, D. H. Ballard, J. Liu, U. Jammalamadaka, R. L. Laforest, R. L. Wahl, and others, "A Projection-Domain Low-Count Quantitative SPECT Method for α-Particle-Emitting Radiopharmaceutical Therapy," *IEEE Transactions on Radiation and Plasma Medical Sciences*, vol. 7, no. 1, pp. 62–74, 2023.

[9] M. Ljungberg and S.-E. Strand, “A Monte Carlo program for the simulation of scintillation camera characteristics,” *Comput Methods Programs Biomed*, vol. 29, no. 4, pp. 257–272, 1989.

[10] M. B. Toossi, J. P. Islamian, M. Momennezhad, M. Ljungberg, and S. Naseri, “SIMIND Monte Carlo simulation of a single photon emission CT,” *J Med Phys*, vol. 35, no. 1, p. 42, 2010.

[11] M. Morphis, J. A. van Staden, H. du Raan, and M. Ljungberg, “Validation of a SIMIND Monte Carlo modeled gamma camera for Iodine-123 and Iodine-131 imaging,” *Heliyon*, vol. 7, no. 6, p. e07196, 2021.